Infrared and dielectric spectroscopy of the relaxor ferroelectric $Sr_{0.61}Ba_{0.39}Nb_2O_6$

2005 J. Phys.: Condens. Matter 17 653

(http://iopscience.iop.org/0953-8984/17/4/008)

INSTITUTE OF PHYSICS PUBLISHING JOURNAL OF PHYSICS: CONDENSED MATTER

J. Phys.: Condens. Matter **17** (2005) 653–666 doi:10.1088/0953-8984/17/4/008

Infrared and dielectric spectroscopy of the relaxor ferroelectric $Sr_{0.61}Ba_{0.39}Nb_2O_6$

E Buixaderas[1], M Savinov[1], M Kempa[1], S Veljko[1], S Kamba[1], J Petzelt[1], R Pankrath[2] and S Kapphan[2]

[1] Institute of Physics, Academy of Sciences of the Czech Republic, Na Slovance 2, 18221 Prague, Czech Republic
[2] Osnabrück University, Fachbereich Physic, Barbarastrasse 7, 49076 Osnabrück, Germany

E-mail: buixader@fzu.cz

Received 27 October 2004
Published 14 January 2005
Online at stacks.iop.org/JPhysCM/17/653

Abstract

The dielectric response of strontium barium niobate with 61% Sr has been studied from kHz to THz frequencies by means of several techniques (IR and time domain THz spectroscopy, the coaxial technique and dielectric spectroscopy) over a wide temperature interval: 20–600 K. A strong dielectric anisotropy is present in all the results. Relaxor ferroelectric properties were detected in $\varepsilon_c^*(T, \nu)$. At very high temperatures a strong relaxation appears in the microwave and THz range, which shifts and broadens to lower frequencies on cooling and then splits into two components. The high frequency one is seen in the THz range at high temperatures and the strong low frequency one weakens below the temperature T_m of the smeared permittivity maximum and broadens extremely in the spectra leaving a constant-loss background at very low temperatures. This relaxation is responsible for the dielectric anomaly near the ferroelectric transition. No anomalies in phonon frequencies were observed, which gives evidence relating to the order–disorder mechanism of the phase transition. The response perpendicular to the polar axis shows anomalous features at low temperatures, which could be connected with the shift of the low frequency limit of a broad dispersion (much weaker than along the polar axis) from the GHz range at 200 K to the kHz range at 40 K. There is no clear evidence of a new phase transition below 100 K suggested by some authors.

1. Introduction

Strontium barium niobate, $Sr_{0.61}Ba_{0.39}Nb_2O_6$ (SBN-61), has attracted much attention due to its relaxor, pyroelectric, dielectric, electro-optical and non-linear optical properties [1, 2]. It crystallizes in the unfilled tetragonal tungsten-bronze structure [3, 4] in which the A_1 site (12-fold correlated site inside the squared channels) is occupied by Sr, the A_2 site (15-fold

correlated site inside the pentagonal ones) by Sr and Ba, and the C site (inside the triangular channels) is empty. This intrinsic disorder in the structure contributes to its excellent dielectric properties [1, 5]. The crystal structure is tetragonal above $T_m \sim 360$ K and shows relaxor ferroelectric behaviour, probably having the centrosymmetric point group $4/mmm$ [6] as in other tungsten bronzes—although an intermediate phase with non-centrosymmetric point group $\bar{4}2m$ can be present just above T_m due to the non-zero gradually disappearing second-harmonic signal [4, 7]. Below T_m a new tetragonal phase appears, with the space group $P4bm$ [3], and the crystal becomes ferroelectric. An incommensurate modulation is present in the crystal with a two-dimensional modulation vector $\mathbf{q} = (1+\delta)/4(\mathbf{a}^* \pm \mathbf{b}^*) + \frac{1}{2}\mathbf{c}^*$ and $\delta = 0.23$ at room temperature [8]. The modulation factor δ does not change appreciably from 300 to 700 K [9]. At low temperatures a new phase transition (PT) to a monoclinic phase was proposed [10] from the analogy with other tungsten bronze structures, but clear evidence for it is still lacking.

The dynamics of the PT was studied by means of Raman spectroscopy for $Sr_xBa_{1-x}Nb_2O_6$ samples with $x = 0.75$ [11], $x = 0.61$ [12] and $x = 0.66$ [13]. New phonon modes were observed below T_m due to the symmetry change, but no clear soft mode was found. Phonon anomalies were seen below 100 K, related to a possible new PT [13]. The IR reflectivity spectrum of SBN-61 (doped with Cu) was studied at room temperature in [14], and a preliminary temperature dependence for IR active modes along the polar axis was reported recently by us [15]. The presence of central peaks at very high temperatures was studied by means of Brillouin scattering [16]; this indicated a thermal switching of polar nanoclusters. Neutron scattering [17] also failed in finding soft modes, but central peaks were discovered in SBN-70 and SBN-45 (with the half-width of $\sim$3 meV) and assigned to the anharmonic hopping motion of Ba/Sr atoms at A_2 sites.

In this paper we report on the dielectric behaviour of SBN-61 for both polarizations from 20 to 600 K using a broad frequency range (from 100 Hz to 67 THz), including Fourier transform IR (FTIR) and time domain THz (TD THz) spectroscopy.

2. Experimental details

The SBN-61 single crystal was grown by the Czochralski method, with a weak doping with Rh (50 ppm). A big bulk crystal ($5 \times 5 \times 8$ mm^3) was cut into several samples of different orientations to enable measurements parallel and perpendicular to the polar axis. Samples were studied by means of FTIR reflectivity, TDTHz transmission spectroscopy (90 GHz–2.5 THz), the high frequency (HF) coaxial technique (1 MHz–1.8 GHz) and low frequency (LF) dielectric spectroscopy (100 Hz–1 MHz).

IR reflectivity measurements were performed on a bulk sample ($4.4 \times 2.4 \times 6.0$ mm^3) with the polar axis along the larger axis using a Fourier spectrometer, Bruker IFS 113v, equipped with two room temperature DTGS pyroelectric detectors as well as a He-cooled (1.5 K) Si bolometer. Room temperature spectra were measured in the range 30–2000 cm^{-1} (1–67 THz) with a resolution of 2 cm^{-1}. For low temperature measurements (down to 10 K) we used a continuous-flow Oxford Optistat CF cryostat with the sample mounted in a He gas bath and the light was polarized by a metal-mesh polarizer deposited on a thin polyethylene foil. For high temperatures (300–570 K) we used a custom-made oven together with a pile-of-plates polarizer made of several polyethylene foils tilted by the Brewster angle. The use of polarizers and optical windows at high and low temperatures reduced the accessible frequency range to 30–620 cm^{-1}.

For dielectric measurements in the HF range three cylindrical samples were cut (of the following heights h and diameters d: $h_1 = 7.5$ mm, $d_1 = 0.4$ mm and $h_2 = 7.5$ mm, $d_2 = 1.0$ mm, with the polar axis parallel to the cylinder axis, and $h_3 = 5.0$ mm, $d_3 = 1.0$ mm,

with the polar axis perpendicular to the cylinder axis). A computer controlled HF dielectric spectrometer equipped with an HP 4291B impedance analyser, a Novocontrol BDS 2100 coaxial sample cell and a Sigma System M18 temperature chamber (operation range 100–570 K) were used. The impedance of the samples with Au electrodes sputtered on the bases of the cylinder was recorded on cooling at the rate 1 K min^{-1}.

TD THz transmission measurements were carried out on a thin polished plane-parallel sample ($5 \times 5 \times 0.1$ mm^3) with orientation (100) in the temperature range 25–700 K, using a polarized electromagnetic field to measure the $\mathbf{E}\|\boldsymbol{c}$ and $\mathbf{E}\perp\boldsymbol{c}$ spectra. A custom-made time domain THz transmission spectrometer was used to obtain the complex dielectric response from 3 to 20 cm^{-1} with a resolution of 0.5 cm^{-1}. An Optistat CF cryostat with Mylar windows (thickness 25 and 50 μm for the inner and outer windows, respectively) was used for measurements down to 25 K. An adapted commercial high temperature cell, Specac P/N 5850, with 1 mm thick sapphire windows was used to heat the sample up to 700 K.

For LF dielectric measurements with the Hewlett-Packard 4192A impedance analyser, gold electrodes were added onto the faces of two plates ($4.5\times6\times0.2\,mm^3$ and $5\times5\times0.1\,mm^3$) with orientations (001) and (100). The samples were heated and cooled in the temperature range of 20–500 K at a rate of 2 K min^{-1} under a measurement field of 5 V cm^{-1}.

3. Results and evaluation

3.1. IR and THz measurements

In order to clarify the IR results concerning the number and symmetry of the phonon modes measured, we present the factor group analysis of the lattice vibrations for SBN, which has so far not been published. Up to now, all references referred to the general analysis for tungsten bronze structure published by Burns [18]. However, the disorder was not taken into account in this structure and the real number of possible modes depends strongly on it. In table 1 we present the group analysis for SBN at room temperature in the ferroelectric phase using the structural data given by Jamieson (for SBN-75) [4] and the more recent data given by Chernaya for SBN-61 [3], compared with the ideal structure. Disorder increases the number of effective atoms in the unit cell and therefore the number of allowed modes. Using Jamieson data [4], we took an effective Ba/Sr atom in site 4c and disorder among O atoms in two sites, resulting in 56 effective atoms and 168 modes, instead of 46 atoms and 138 modes (see table 1). Chernaya's data [3] situate Ba at 4c sites but some Sr at 8d sites which gives 64 effective atoms and 192 modes, distributed in the symmetries shown in the table 1.

The IR reflectivity spectra for both the polarizations, including the THz reflectivity calculated from the THz transmission, are shown in figure 1 together with the corresponding fits at selected temperatures. All experimental reflectivity spectra were fitted with the generalized oscillator model of the dielectric function [19]:

$$\varepsilon^*(\nu) = \varepsilon'(\nu) - \mathrm{i}\varepsilon''(\nu) = \varepsilon_\infty \prod_{i=1}^{n} \frac{\nu_{\mathrm{LO}i}^2 - \nu^2 + \mathrm{i}\nu\gamma_{\mathrm{LO}i}}{\nu_{\mathrm{TO}i}^2 - \nu^2 + \mathrm{i}\nu\gamma_{\mathrm{TO}i}}, \tag{1a}$$

$$\Delta\varepsilon_i = \frac{\varepsilon_\infty}{\nu_{\mathrm{TO}i}^2} \frac{\prod_k (\nu_{\mathrm{LO}k}^2 - \nu_{\mathrm{TO}i}^2)}{\prod_{k\neq i} (\nu_{\mathrm{TO}k}^2 - \nu_{\mathrm{TO}i}^2)}, \tag{1b}$$

where ε_∞ is the permittivity at frequencies much higher than all polar phonon frequencies, $\nu_{\mathrm{TO}i}$ and $\nu_{\mathrm{LO}i}$ are the transverse and longitudinal frequencies of the ith phonon mode and $\gamma_{\mathrm{TO}i}$ and $\gamma_{\mathrm{LO}i}$ their respective damping constants.

Looking into figure 1, a pronounced anisotropy between the two polarizations of the IR spectra is observed. In the paraelectric phase, 6 A_{2u} (for the $\mathbf{E}\|\boldsymbol{c}$ polarization) and 12E_u

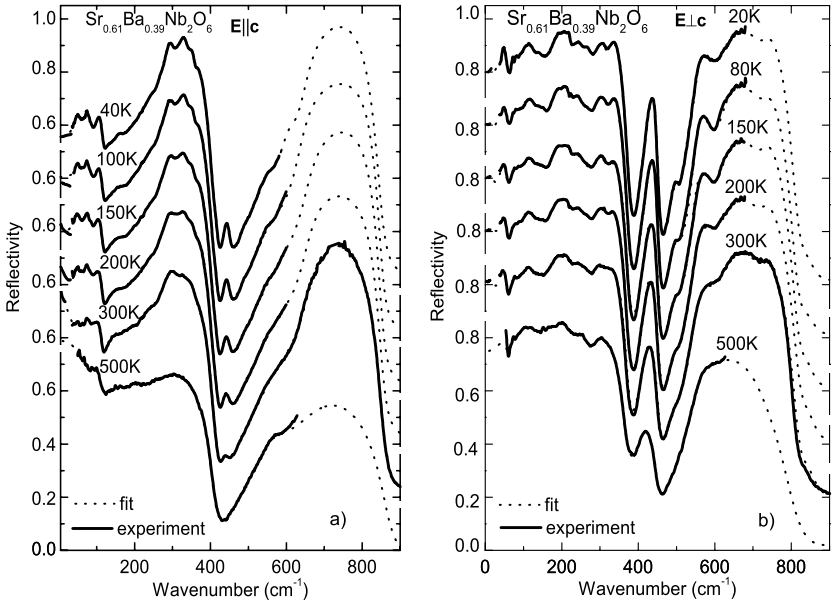

Figure 1. IR and THz reflectivity spectra of SBN-61 together with their fits (dotted curves) at several temperatures for (a) $\mathbf{E}\|c$ and (b) $\mathbf{E}\perp c$ polarizations.

Table 1. Factor group analysis for SBN, taken into account different x-ray data [3, 4] at room temperature, together with the theoretical analysis [18].

Paraelectric, D_{4h} $4/mmm$, $Z = 5$		Ferroelectric, C_{4v} $Z = 5$, $P4bm$ A_{2u}–A_1 $\mathbf{P}_s \parallel (001)$	
Burns [18]	Burns (ideal structure) [18]	Jamieson's data [4]	Chernaya's data [3]
$10A_{1g}$ (*aa bb cc*) $9A_{2u}$ (*c*)	$19A_1$ (*c*, *aa bb cc*)	$23A_1$ (*c*, *aa bb cc*)	$26A_1$ (*c*, *aa bb cc*)
$10B_{1g}$ (*aa bb*) $4B_{2u}$ (—)	$14B_1$ (—, *aa bb*)	$18B_1$ (—, *aa bb*)	$21B_1$ (—, *aa bb*)
$10E_g$ (*ac bc*) $26E_u$ (*a*, *b*)	36E (*a b*, *ac bc*)	43E (*a b*, *ac bc*)	49E (*a b*, *ac bc*)
$5A_{1u}$ (—) $10A_{2g}$ (—)	$15A_2$ (—)	$19A_2$ (—)	$22A_2$ (—)
$8B_{1u}$ (—) $10B_{2g}$ (*ab*)	$18B_2$ (—, *ab*)	$22B_2$ (—, *ab*)	$25B_2$ (—, *ab*)
138 modes	138(−3 acoustic) modes 46 atoms	168(−3) modes 56 effective atoms: 4 O + 1 Nb, site 8*d* 2 O + 1 Ba/Sr, site 4*c* 1 Nb, site 2*b* 1 Sr, site 2*a*	192(−3) modes 64 effective atoms: 4 O + 1 Sr + 1 Nb, site 8*d* 2 O + 1 Ba, site 4*c* 1 Nb, site 2*b* 1 Sr, site 2*a*

(for the $\mathbf{E}\perp\boldsymbol{c}$ polarization) optical modes were fitted. Theoretical group analysis gives a result of $8A_{2u}$ (*c*) and $25E_u$ (*a*, *b*) optical modes, with the acoustic branches subtracted (see table 1). In the ferroelectric phase, at the lowest temperature, 18 A_1 and 24 E modes were fitted. However, 25 A_1 (*c*) and 48 E (*a*, *b*) optical modes are predicted (see table 1). In our spectra

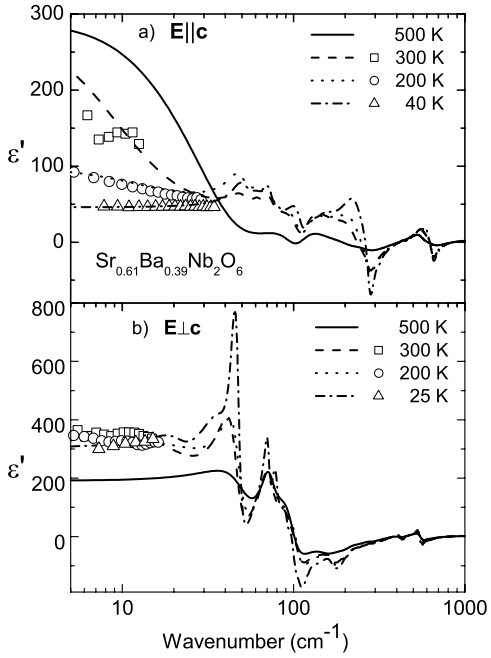

Figure 2. The temperature dependence of the permittivity obtained from the fit of the IR reflectivity for SBN-61 single crystal together with experimental THz data: (a) $\mathbf{E}\|\boldsymbol{c}$ and (b) $\mathbf{E}\perp\boldsymbol{c}$ polarization.

we see a lower number of modes due to the small strength and overlap of some of them. No pronounced anomalies in the mode frequencies were observed on lowering the temperature, which speaks in favour of an order–disorder mechanism for the ferroelectric transition. In table 2 we present a list of mode parameters (transverse frequency ν_T, transverse damping γ_T and dielectric strength $\Delta\varepsilon$, calculated from the formula (1*b*), in paraelectric and ferroelectric phases for both polarizations.

The permittivity and losses calculated from the previous fits are presented together with the experimental THz points in figures 2 and 3, for the two polarizations, respectively, at selected temperatures. The permittivity in the polar axis due to the phonon contribution is rather low ($\varepsilon'_c \sim 50$), as in other tungsten bronze materials [20], but another excitation is present below the phonon frequencies which enhances the ε' values in the THz range (see figure 2(a)). On cooling, this excitation vanishes and the THz values agree with the phonon contribution. Such an effect is not seen for the $\mathbf{E}\perp\boldsymbol{c}$ polarization (figure 2(b)), where below phonons a central mode (CM) was used to fit the THz data in the whole temperature range ($\Delta\varepsilon_{CM} \sim 100$). The phonon contribution is $\varepsilon'_a \sim 200$, which is much higher than in the polar direction. It is a common feature of the tungsten bronze structures that for the perpendicular polarization the reflection bands are very wide and intense and, therefore, their dielectric contribution to the permittivity is higher. In figure 3 the loss spectra are depicted at different temperatures. Each peak corresponds to a phonon mode. On cooling, phonons are better distinguished and in the low frequency range the CMs are seen as broad peaks. The most intense one is for the polar axis polarization at high temperatures (figure 3(a)).

We note that figures 2 and 3 do not show any THz data above T_m because in the transmission THz experiment the sample was translucent only below T_m. In the relaxor paraelectric phase the sample became almost opaque up to 700 K, but at this temperature the THz signal was

Table 2. Parameters of the IR phonons of SBN-61 for both the polarizations in paraelectric and ferroelectric phases (ν_T and γ_T in cm^{-1}).

SBN-61 $\mathbf{E}\|\boldsymbol{c}$ A_1 modes					
Ferroelectric phase (100 K)			Paraelectric phase (400 K)		
ν_T	γ_T	$\Delta\varepsilon$	ν_T	γ_T	$\Delta\varepsilon$
51.2	14.9	10.0			
63.5	10.4	1.9			
72.9	12.5	2.9			
86.3	15.9	1.2			
107.3	21.8	7.3	104.6	34.6	7.9
132.8	37.0	2.4	135.9	99.2	21.7
153.4	43.5	1.8			
234.0	75.4	15.4	211.3	101.8	4.8
278.3	38.8	1.0	256.5	96.3	6.4
312.2	35.7	0.6			
347.1	24.0	0.1			
358.0	23.8	0.06			
409.9	30.8	0.03			
442.2	21.7	0.1			
553.9	69.6	0.8	551.9	93.5	1.6
604.6	45.4	0.7			
638.6	49.4	1.2	649.9	136.3	1.5
886.4	51.4	0.01			
SBN-61 $\mathbf{E}\perp\boldsymbol{c}$ E modes					
39.3	14.2	45.5			
46.8	6.4	115.8	47.0	28.9	126.1
62.2	12.5	3.4			
71.4	5.7	13.7	69.6	22.7	38.2
79.0	8.1	9.8			
92.0	10.9	14.7			
99.9	14.3	33.6			
107.6	14.5	14.0	103.4	37.9	50.0
136.8	28.1	4.9			
171.4	30.4	4.4	164.0	61.2	12.7
187.1	25.0	0.2			
209.3	42.4	4.0	203.8	60.0	4.8
226.9	24.1	1.2	224.0	51.4	2.3
263.2	35.3	0.3			
287.3	40.4	1.3	283.6	41.7	0.7
324.4	26.9	0.2	318.6	67.5	0.4
410.7	28.8	0.2	412.9	55.2	1.1
427.8	27.1	0.6			
498.8	24.3	0.3	487.0	99.9	0.6
529.9	24.2	0.4			
549.8	23.4	1.6	548.6	42.0	1.7
614.3	70.9	0.5	620.8	87.5	0.3
728.6	61.2	0.01	727.2	92.4	0.01
839.2	50.7	0.01			

recovered. This effect could be due to the presence of an intense CM in the THz range only in this interval of temperatures (350–600 K). Therefore the $\mathbf{E}\|\boldsymbol{c}$ THz data from 400 to 600 K are not shown and should be treated as only qualitative.

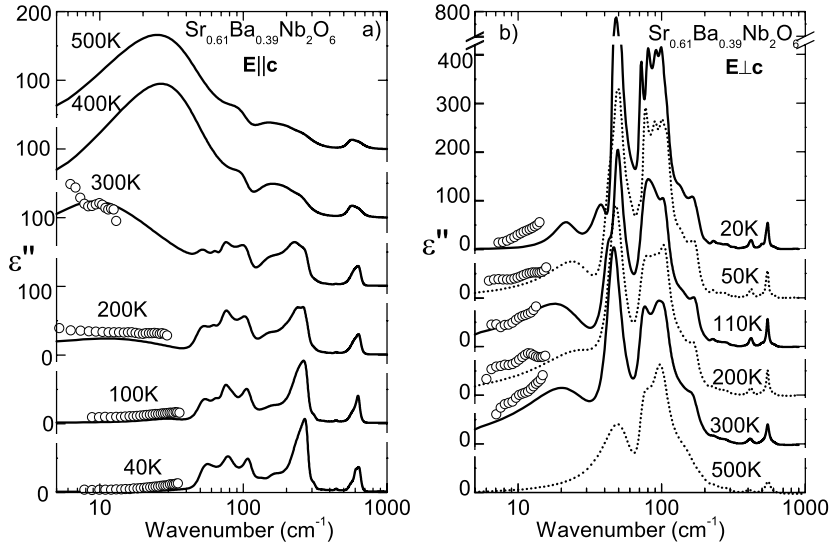

Figure 3. The temperature dependence of the losses obtained from the fit of the IR reflectivity for SBN-61 single crystal together with experimental THz data: (a) $\mathbf{E}\|\boldsymbol{c}$ and (b) $\mathbf{E}\perp\boldsymbol{c}$ polarization.

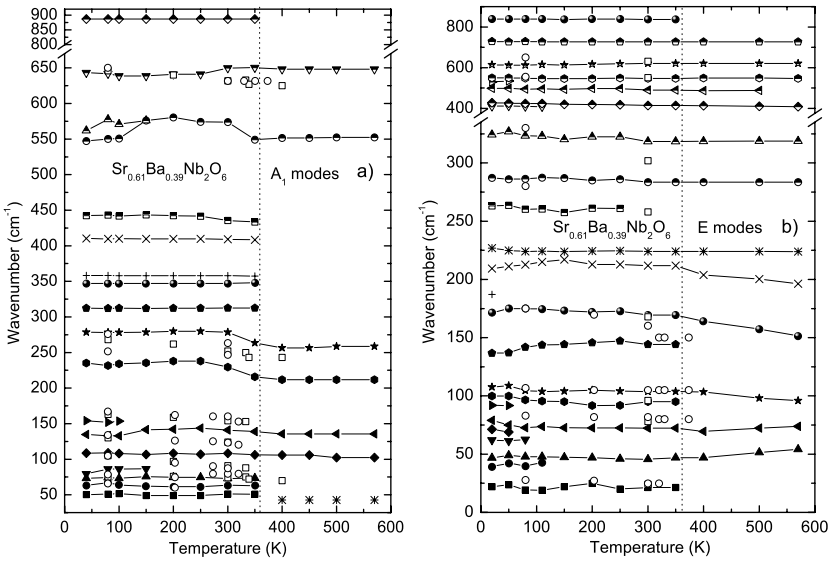

Figure 4. The temperature dependence of the mode frequencies obtained from the fits for SBN-61 single crystal (black symbols) together with Raman modes (open symbols) from [11, 12]: (a) $\mathbf{E}\|\boldsymbol{c}$ and (b) $\mathbf{E}\perp\boldsymbol{c}$ polarization.

Figure 4 shows the temperature dependence of the transverse phonon frequencies for both A_1 and E modes. The PT at 360 K is clearly seen from the appearance of new modes in the ferroelectric phase. For comparison we have plotted also Raman modes found in the literature [11, 12], which mostly coincide in the ferroelectric phase. From this picture it is clearly seen that there is no soft optical mode connected with the ferroelectric PT.

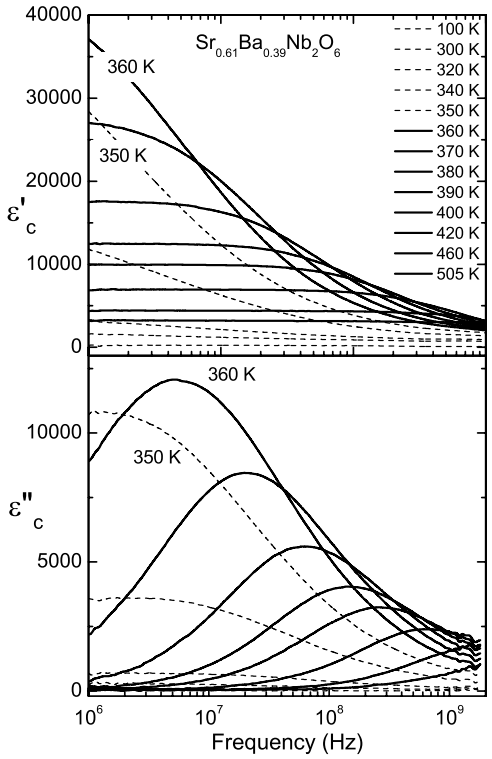

Figure 5. Frequency dependences of the permittivity ε_c' and losses ε_c'' obtained in the HF range (coaxial technique) for SBN-61.

3.2. HF and LF dielectric measurements

HF data show that a huge relaxation crosses this spectral range, which is responsible for the extremely high value of the permittivity. In figure 5 we present the permittivity and loss spectra measured in the HF experiment for selected temperatures versus frequency for the polarization parallel to the *c* axis. Following the maxima in the losses one can see that the relaxation appears at high temperatures; the left wing is seen already at 500 K, and on cooling it shifts to lower frequencies and increases in intensity down to $T_m \sim 360$ K. Then it starts to lose its strength, but still slows down to ∼200 K, where it seems to stop and on further cooling disappears from the spectra. This behaviour is in agreement with the one described in [21]. In figure 6 we show the temperature dependence of the mean relaxation frequency ν_R taken from the ε'' maxima in figure 5 and its contribution $\Delta\varepsilon$ to the permittivity. The frequency shifts from several GHz near 500 K down to 1 MHz at 350 K where it almost freezes out. A simple fit with the classical slowing down, $\nu_R = a(T - T_c)$, gives the values $a = (24 \pm 1) \times 10^6$ Hz K^{-1} and $T_c = (388 \pm 2)$ K, but to obtain an accurate fit a Vogel–Fulcher model was used, $\nu = \nu_\infty \exp(-E_0/k(T - T_{VF}))$, where ν_∞ is the saturation frequency, E_0 the activation energy and T_{VF} the freezing temperature. The fit parameters found for this excitation were $\nu_\infty = (14.0 \pm 0.5) \times 10^9$ Hz, $E_0/k = (270 \pm 4)$ K^{-1} and $T_{VF} = 330$ K. The dielectric strength of this relaxation shows that it is responsible for the huge dielectric anomaly at T_m.

The LF dielectric measurements revealed the strong peak due to the relaxor–ferroelectric transition at ∼360 K and an additional feature at low temperatures, better seen in loss spectra. A Curie–Weiss fit, $\Delta\varepsilon = C/(T - T_0)$, at 100 kHz gives $C = 4.35 \times 10^6$ K^{-1} and $T_0 = 355$ K above T_m, and $C = -2.86 \times 10^4$ K^{-1} and $T_0 = 330$ K below it. However, the low temperature data are influenced by the second dielectric anomaly near 100 K. In figure 7 we show the loss

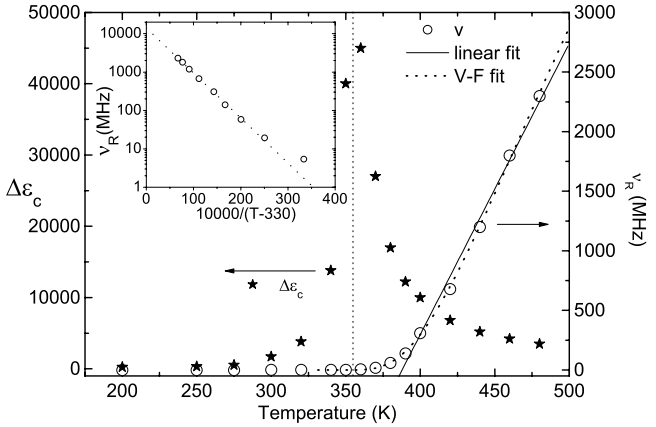

Figure 6. The dielectric contribution $\Delta\varepsilon$ and mean frequency ν_R of the main HF excitation taken from the ε'' maxima in figure 5. Solid line: the fit with the linear law. Dashed line: the fit with the Vogel–Fulcher law. The inset shows ν_R in a Vogel–Fulcher plot.

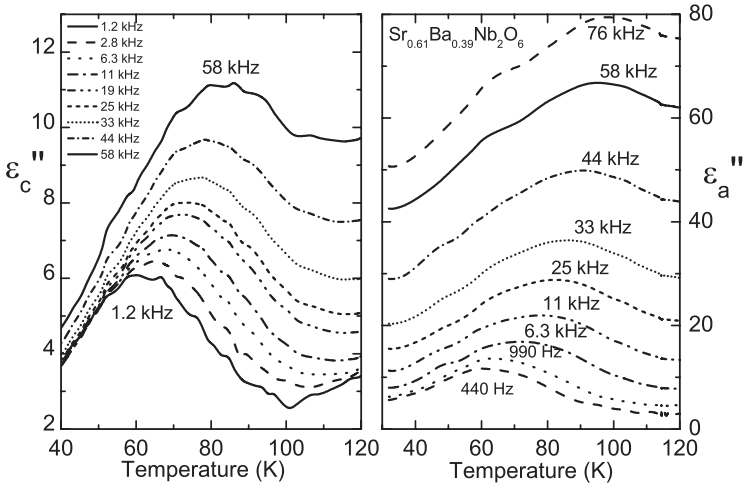

Figure 7. The temperature dependence of the dielectric losses in SBN-61 in the LF range measured at several frequencies.

spectra at both polarizations below 120 K, displaying a peak which shifts to lower temperatures on decreasing frequency. This effect was related to the presence of a new PT [10].

Temperature dependences for both permittivities ε_c' and ε_a' are depicted in figure 8 for various frequencies from kHz to THz, including also the total phonon contribution $\sum \Delta\varepsilon_{\rm ph}$. In figure 8(a) the huge permittivity maximum connected with the ferroelectric PT is seen from GHz down to kHz, showing relaxor character: the ε' maximum strongly shifts with frequency, mainly in the HF range. THz data show a weak temperature dependence, related to the presence of the high frequency wing of the relaxation in the microwave range. The contribution of phonons is small ($\sum \Delta\varepsilon_{\rm ph} \sim 50$) and constant, but on heating an extra contribution is needed to achieve the THz values, due to the influence of a CM, which could be assigned to the dynamics of the polar clusters.

In figure 8(b) we show data for perpendicular to the polar axis. There is a small leakage of the ε_c' maximum at $T_{\rm m}$, probably due to a small misorientation of the sample. The THz

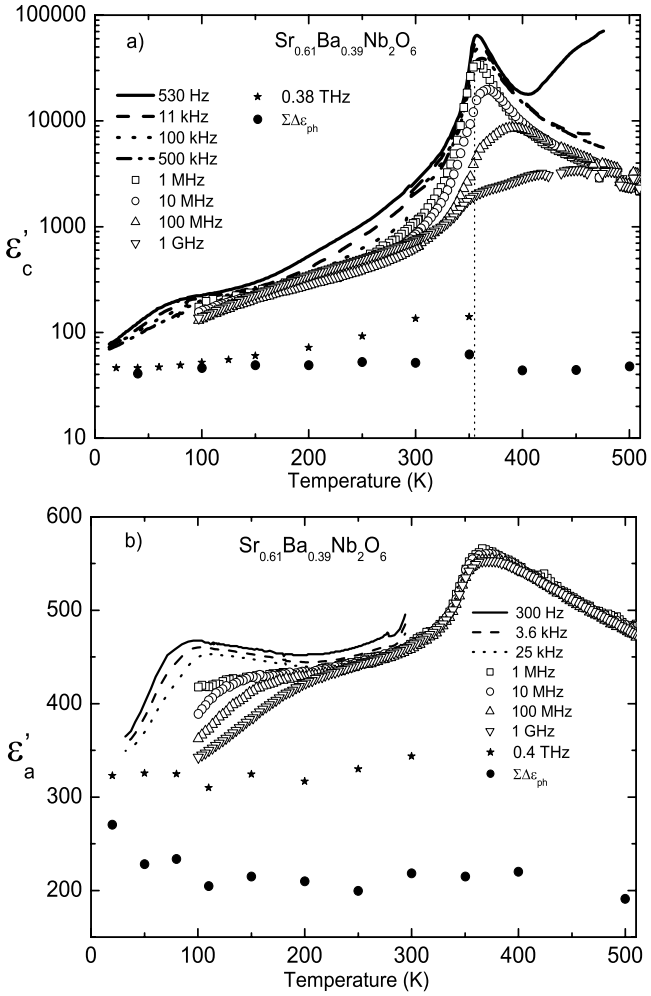

Figure 8. The measured permittivity at various frequencies and the dielectric contribution of phonons; (a) $\mathbf{E}\|c$—note the logarithmic scale—and (b) $\mathbf{E}\perp c$ polarization.

data and phonon contribution are temperature independent, $\varepsilon'_{\mathrm{THz}} \sim 300$ and $\sum \Delta\varepsilon_{\mathrm{ph}} \sim 200$ respectively, so a CM is responsible for the difference, $\Delta\varepsilon_{\mathrm{CM}} \sim 100$. On cooling, HF and LF data show that the anomaly shifts from 200 K, at GHz frequencies, to ∼80 K, at 300 Hz, but it is not clear whether it could be due to some trace of a new PT or to dipolar glass behaviour. This anomaly is better seen in losses (figure 7) at lower frequencies and temperatures.

4. Discussion

The absence of an optical soft mode in SBN-61 confirms the order–disorder type of the ferroelectric PT. However, anomalies in the behaviour of the low frequency relaxations were found. The most striking anomaly is the slowing down of the HF relaxation together with the change in its dielectric strength shown in figure 6. To better analyse the dielectric behaviour of SBN-61 we plot all dielectric data in the polar direction in figure 9, where permittivity and

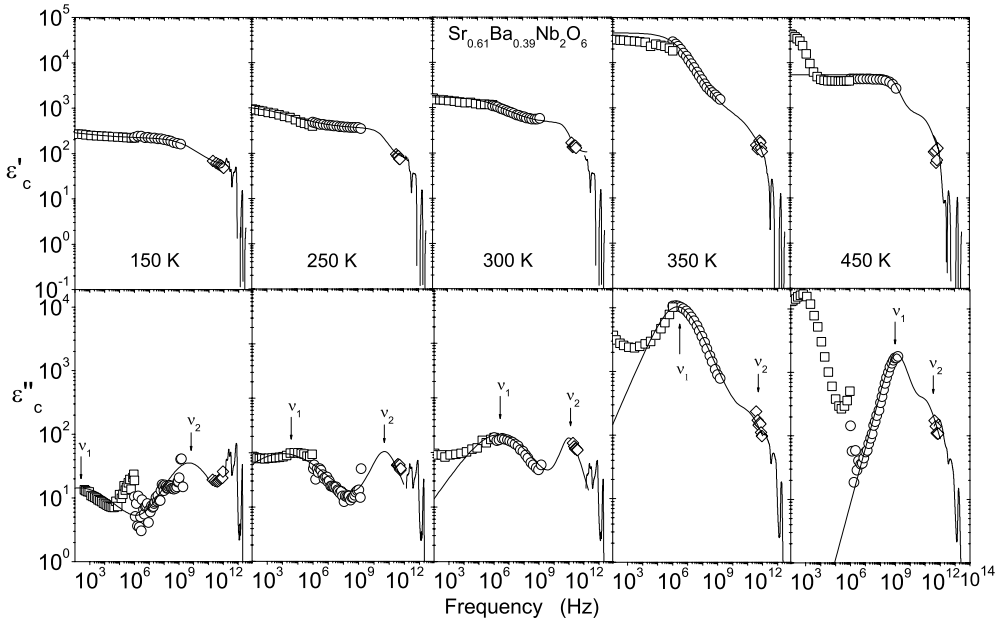

Figure 9. The complex dielectric function ε_c^* for SBN-61 crystal at various temperatures. Note the logarithmic scales.

loss spectra are shown for selected temperatures, from 10^2 to 10^{14} Hz. Experimental data are marked by open symbols together with their fits (solid curves). IR fits (10^{12}–10^{14} Hz) were taken using the model with equation (1) and dielectric fits (10^2–10^{12} Hz) were performed using the Cole–Cole model

$$\varepsilon^*(\nu) = \frac{\Delta\varepsilon}{1 + (\mathrm{i}\nu/\nu_0)^{1-\alpha}}, \tag{2}$$

where $\Delta\varepsilon$ is the dielectric contribution of the relaxation, ν_0 the mean relaxation frequency and α a real index between 0 and 1.

Two extra modes were needed to account for the difference between the IR and THz data and the HF and LF values. In $\varepsilon(\nu)''$ a broad peak crosses the spectra on cooling from several GHz to kHz. This is the excitation shown in figures 5 and 6, responsible for the high values of the permittivity and contributing to the ferroelectric PT. In figure 9 we can follow the evolution of this excitation (ν_1) to lower temperatures; it shows that on cooling the relaxation slows down and broadens. At very low temperatures (50 K), not shown in the figure, the presence of a wide interval with low and almost frequency independent losses suggests the presence of a very broad distribution of relaxations.

The secondary excitation (ν_2) of higher frequency develops on cooling, probably below 500 K, and shifts from the THz to the GHz range. This is connected with the high absorption in the THz range above T_m. From the analogy with classical relaxor ferroelectrics, it can be expected that, on heating, the relaxation frequency will increase, merge with phonons in the form of a CM and finally disappear above the Burns temperature, where the polar clusters vanish (probably above 600 K).

The low frequency increase in $\varepsilon^*(\nu)$ at high temperatures (figure 9) is obviously connected with the finite conductivity of our sample.

The parameters of the Cole–Cole fits in the polar direction are presented in figure 10. The figure shows the temperature dependences of the mean relaxation frequency ν_0, dielectric

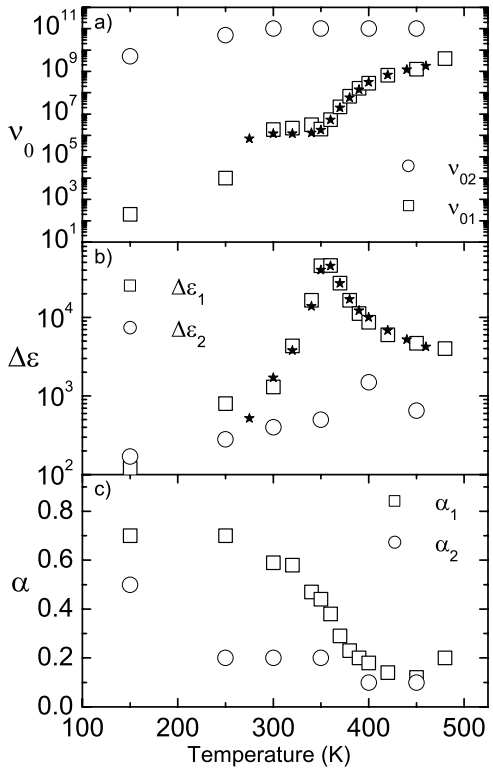

Figure 10. Temperature dependences of the parameters from the Cole–Cole fit shown in figure 9. Black stars correspond to the previous estimation in figure 6 (present for comparison).

contribution $\Delta\varepsilon$ and α. In figure 10(a) we can follow the temperature behaviour of the frequency. We suppose that at high temperatures $T > 500$ K there is an intense excitation (CM-like) in the THz range. On cooling, near 450 K, this relaxation splits into two components: a weaker one (ν_2) located in the THz range and a stronger one (ν_1) in the GHz range, which looses intensity gradually and slows down. The CM ν_2 is almost frequency independent; it just approaches the GHz range at low temperatures, and its dielectric contribution is much weaker, not sufficient to explain the dielectric anomaly at the ferroelectric PT (figure 10(b)). In contrast, the relaxation ν_1 slows down towards T_m, and almost freezes in the MHz range near the PT. This is the broad relaxation detected in HF measurements—results from figure 6 are shown in figures 10(a) and (b) by full stars for comparison. However, the freezing is not complete and for $T < 300$ K the mean frequency ν_{01} decreases further. The parameter α, which measures the deviation of the relaxation from the Debye behaviour ($\alpha = 0$), can be followed in figure 10(c). It can be seen from the almost Debye character at $T > 400$ K ($\alpha_1 \sim 0.12$) that the relaxation broadens strongly ($\alpha_1 \sim 0.7$ at 250 K). The low frequency end of this broad relaxation probably slows down and accounts for the low temperature dielectric anomaly seen in figures 7 and 8.

Figure 11 shows the whole dielectric spectra for the $\mathbf{E}\perp\boldsymbol{c}$ polarization for selected temperatures, from 10^2 to 10^{14} Hz, together with their fits. There are two weak excitations below the phonons. The first one is a CM present in the THz range ($\Delta\varepsilon_{CM} \sim 100$, $\nu_{CM} \sim 25\ \mathrm{cm}^{-1}$) and its parameters remain almost constant down to low temperatures. Below, there is an additional dispersion. At room temperature it is located between the GHz and THz ranges ($\Delta\varepsilon \sim 100$, $\nu_0 \sim 10^{10}$ Hz, $\alpha \sim 0.1$). On cooling, it shifts to lower frequencies

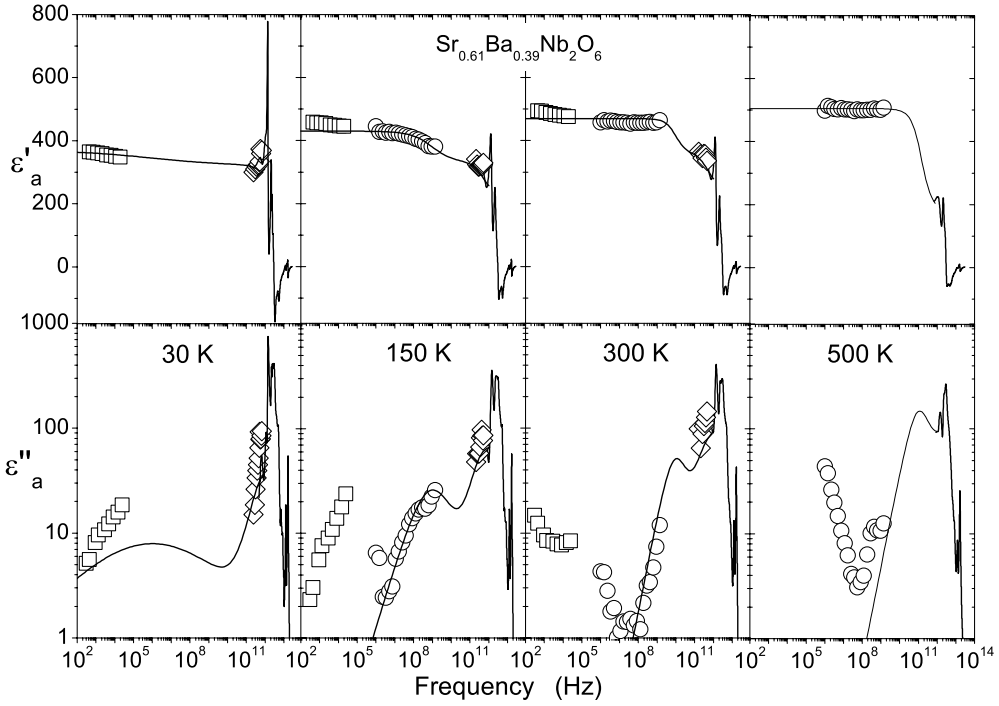

Figure 11. The complex dielectric function ε_a^* for SBN-61 crystal at various temperatures. Note the logarithmic scales.

and broadens; at 150 K the parameters are $\Delta\varepsilon \sim 100$, $\nu_0 \sim 10^9$ Hz and $\alpha \sim 0.4$. For the lowest temperature its estimated parameters are $\Delta\varepsilon \sim 50$, $\nu_0 \sim 10^6$ Hz and $\alpha \sim 0.8$, which shows that again we deal with a broad relaxation. Loss data below 1 MHz were not taken into account during the fit, but they show that an extra relaxation could be present there, although very weak, because its contribution to the permittivity is very small. The low temperature anomaly of glassy-like type (seen in figures 7 and 8) could be caused by the slowing down of the low frequency end of this relaxation on cooling. It is possible to assume also a change in the modulation factor δ of the SBN, to reach a lock-in phase at low temperatures. Up to now, no measurements of this parameter have been made below room temperature. A low temperature transition to a monoclinic phase is typical for tungsten bronze structures with the appearance of a new polarization component. The only experimental support of this transition in SBN-61 was published in [10]. For SBN-66, anomalies in the temperature dependence of the Raman mode frequencies and intensities were seen below 80 K [11]. Our IR data, however, did not show any appreciable anomaly. Therefore diffraction studies are needed to elucidate the behaviour of the modulation and existence of possible PTs in SBN-61 at low temperatures.

The incommensurate modulation of SBN-61 was found to be associated with some O atoms, and also with Ba and Sr ordering at sites 4c [8]. Positional modulation of Ba, Sr together with the modulation of the atomic positions of Sr and Ba in A_2 sites is the cause of random fields in the octahedra framework. Random fields create polar agglomerates embedded in the $(Nb_2O_6)_n$ matrix. Above T_m the agglomerates take the form of polar nanoclusters and they evolve into ferroelectric grains and domains at T_m. However, random fields are still present below T_m in the ferroelectric phase due to the discommensuration and this could cause the broadening of the relaxations detected.

5. Conclusions

The dielectric behaviour of a SBN-61 single crystal has been studied from 10^2 to 10^{14} Hz by several experimental techniques. No soft phonon mode was found; therefore the ferroelectric PT can be assigned as order–disorder type. A strong relaxation below polar phonon frequencies plays an essential role in the ferroelectric and relaxor behaviour. Above the Burns temperature it is assumed to be located in the THz range. On cooling, it splits into two components: a CM in the GHz range and another strong lower frequency relaxation. The frequency and dielectric strength of the CM remain almost temperature independent, whilst the other relaxation slows down and weakens. The latter relaxation is responsible for the ferroelectric transition: its strength grows on approaching the PT, showing a maximum at $T_m \sim 360$ K. Its frequency obeys the Vogel–Fulcher rule, slowing down above T_m with a freezing temperature near 330 K. On further cooling, its slowing down becomes weaker and the relaxation substantially broadens. Both relaxations can be assigned to dynamics of polar clusters and dynamic disorder of Sr and Ba atoms at A_2 sites.

The dielectric anomaly at low temperatures is caused by slowing down of the low frequency end of a broad relaxation, which could be a consequence of a lock-in into a new commensurate ferroelectric phase. Diffraction and Raman scattering experiments at low temperatures are scheduled, to check the last hypothesis.

Acknowledgments

This work was supported by the Academy of Sciences of the Czech Republic (project A1010213), by the Grant Agency of the Czech Republic (project No 202/04/0993) and by DFG-KA 501/8-1 and DFG 436 TSE 17/7/02.

References

[1] Glass A M 1969 *J. Appl. Phys.* **40** 4699
[2] Ewbanks M D, Neurgaonkar R R and Cory W K 1987 *J. Appl. Phys.* **62** 374
[3] Chernaya T S, Maksimov B A, Verin I V, Ivleva L I and Simonov V I 1997 *Kristallografiya* **42** 421
[4] Jamieson P B, Abrahams S C and Bernstein J L 1968 *J. Chem. Phys.* **48** 5048
[5] Dec J, Kleemann W, Woike T and Pankrath R 2000 *Eur. Phys.* B **14** 627
[6] Oliver J R, Neurgaonkar R R and Cross L E 1988 *J. Appl. Phys.* **64** 37
[7] Lehnen P, Dec J, Kleemann W, Woike T and Pankrath R 2000 *Ferroelectrics* **240** 281
[8] Woike T, Petricek V, Dusek M, Hansen N K, Fertey P, Lecomte C, Arakcheeva A, Chapuis G, Imlau M and Pankrath R 2003 *Acta Crystallogr.* B **59** 28
[9] Balagurov A M, Prokert F and Savenko B N 1987 *Phys. Status Solidi* **103** 131
[10] Xu Y, Li Z, Wang H and Chen H 1989 *Phys. Rev.* B **40** 11902
[11] Rustamov K S, Gorelik V S, Kuzminov Y S, Peregudov C V and Sushchinskyy M M 1976 *Fiz. Tverd. Tela* **18** 3416
[12] Wilde R E 1991 *J. Raman Spectrosc.* **22** 321
[13] Faria J L B, Freire P T C, Ayala A P, Melo F E A, Mendes Filho J, Paschoal C W A, Santos I A and Eiras J A 2003 *J. Raman Spectrosc.* **34** 826
[14] Xia H R, Wang C J, Yu H, Chen H C and Song Y Y 1996 *Cryst. Res. Technol.* **31** 889
[15] Buixaderas E, Kempa M, Veljko S, Savinov M, Kamba S, Petzelt J and Pankrath R 2005 *ECAPD7 Proc. Ferroelectrics* at press
[16] Jiang F M, Ko J H and Kojima S 2002 *Phys. Rev.* B **66** 184301
[17] Prokert F 1982 *Phys. Status Solidi* b **113** 239
[18] Burns G, Giess E A, O'Kane D F, Scott B A and Smith A W 1970 *J. Phys. Soc. Japan* (Suppl.) **28** 153
Burns G, Axe J D and O'Kane D F 1969 *Solid State Commun.* **7** 933
[19] Gervais F 1983 *Infrared and Millimeter Waves* vol 8, ed K J Button (New York: Academic) chapter 7, p 279
[20] Buixaderas E, Porokhonskyy V, Pashkin A, Savinov M and Petzelt J 2002 *Eur. Phys. J.* B **30** 319
[21] Baldenkov A V, Buzin I M, Morozov N A and Rukabishnikov A I 1981 *Fiz. Tverd. Tela* **23** 2376